Application and Modeling of GaN HEMT in 1MHz Large Signal Bandwidth Power Supply for Radio Frequency Power Amplifier

D. Čučak, M. Vasić , O. Garcia , J. Oliver , P. Alou , J. A. Cobos , M. Tadjer , F. Calle , F. Benkhelifa , R. Reiner , P. Waltereit , S. Müller

Abstract— **In this paper, implementation and testing of non-commercial GaN HEMT in a simple buck converter for envelope amplifier in ET and EER transmission techniques has been done. Comparing to the prototypes with commercially available EPC1014 and 1015 GaN HEMTs, experimentally demonstrated power supply provided better thermal management and increased the switching frequency up to 25MHz. 64QAM signal with 1MHz of large signal bandwidth and 10.5dB of Peak to Average Power Ratio was generated, using the switching frequency of 20MHz. The obtained efficiency was 38% including the driving circuit and the total losses breakdown showed that switching power losses in the HEMT are the dominant ones. In addition to this, some basic physical modeling has been done, in order to provide an insight on the correlation between the electrical characteristics of the GaN HEMT and physical design parameters. This is the first step in the optimization of the HEMT design for this particular application.**

I. INTRODUCTION

Nowadays, the radio link design is aiming high peak data rates for high quality multimedia applications such as video, audio, animation, etc. In order to provide these services, more complex modulations and larger bandwidths are required. An actual bottleneck of these radio base stations is their power consumption and low efficiency caused by the poor efficiency of a linear power amplifier, employed in the signal transmission.

There are a lot of techniques that are used in order to enhance the efficiency of a signal transmission: Chireix-outphasing [1], [2], stage switching and bypassing applying adaptive gate switching, Doherty technique [3], Envelope Tracking (ET) [4]-[6] and Envelope Elimination and Restoration (EER) or Kahn's Technique presented in Fig. 1 [7]-[9]. The last two aforementioned techniques are currently being used in a number of applications where efficiency is critical. ET and EER are both based on the voltage modulation at the output of the power supply for Radio Frequency Power Amplifier (RFPA). The modulation is performed according to the signal's envelope and it is done through the Envelope Amplifier (EA) which can be realized either as a stand-alone DC/DC converter or one in parallel with the linear regulator [8]. In this work, a simple buck was a chosen topology for the switching part of EA, using non-commercial GaN HEMT.

The goal of this paper is to make the comparison with the results obtained by applying commercially available EPC1014 and 1015 GaN HEMTs and to increase the large signal bandwidth processed by the switching part of the EA in the case of [8]. Also, some basic physical modeling has been done in order to provide the correlation between electrical and physical parameters of the HEMT.

II. CHARACTERIZATION OF THE DEVICE

The GaN HEMT that was applied as a switching device in this work was designed and fabricated in Fraunhofer Institute for Applied Solid State Physics (IAF). It is rated for 100V and 27A and is a normally-on device with the threshold voltage approximately equal to -2V. The measurement of the threshold voltage for constant V_{ds} bias equal to 1V is presented in Fig. 2.

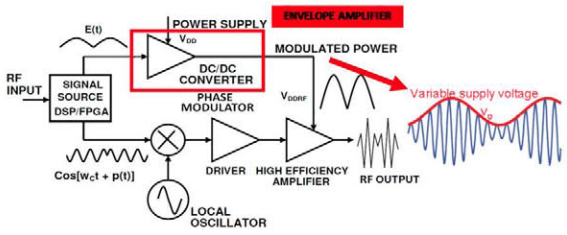

Figure 1. Block Scheme of Kahn Technique Transmitter

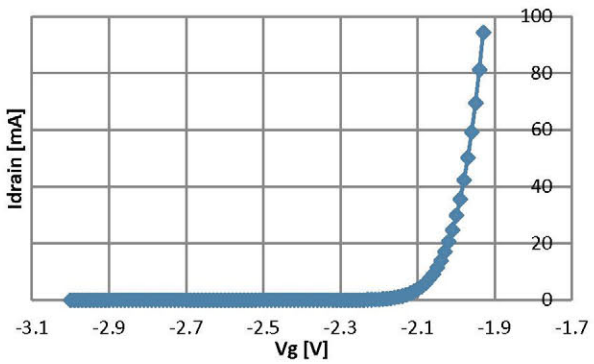

Figure 2. Measured threshold voltage of the HEMT

The physical parameters of the tested device are presented in Table 1. W_g, L_g present the gate width and length respectively, L_{sd} and L_{gd} are the source-to-drain and gate-to-drain distances, m is the mole fraction of Al in $Al_mGa_{(1-m)}N$ layer, d_{AlGaN} is the thickness of AlGaN layer, ε_{AlGaN} is the dielectric permittivity of AlGaN and μ_n is the Hall's mobility of electrons in 2DEG, which is formed in the quantum well at the GaN/AlGaN heterojunction. The cross section of the device is presented in Fig. 3 while the triangular quantum well at the AlGaN/GaN heterojunction is presented in Fig. 4.

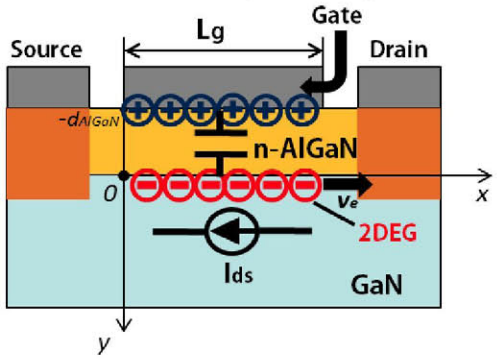

Figure 3. Cross section of the GaN HEMT

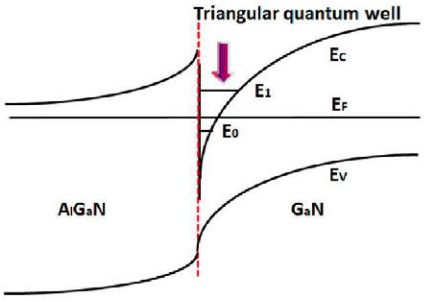

Figure 4. Energy band-diagram of an isolated AlGaN/GaN HEMT in equilibrium

In order to estimate the dependence of on-resistance and input capacitance on the gate-bias voltage and make comparison with the measured values, it is necessary to model the sheet carrier charge density dependence on the gate voltage, $n_{sheet}(V_g)$. Implementation of the model from [10] gives the curve presented in Fig. 5. From this curve it can be seen that for gate voltage approximately equal to 1.4V, sheet density starts to saturate. This phenomenon is well known in the literature [11, 13] and can be explained by analyzing the energy band diagram of the heterojunction (Fig. 6). In this figure, we see that electron quasi-Fermi level, E_{Fn}, inside the AlGaN layer will approach the bottom of the conduction band at large gate voltages and cause a significant transfer of electrons into the AlGaN layer. This means that a parallel MESFET conduction path in AlGaN layer is formed, with significantly lower mobility of electrons. In addition to that, AlGaN has many defects so part of these electrons will be trapped inside and will not contribute to the device current.

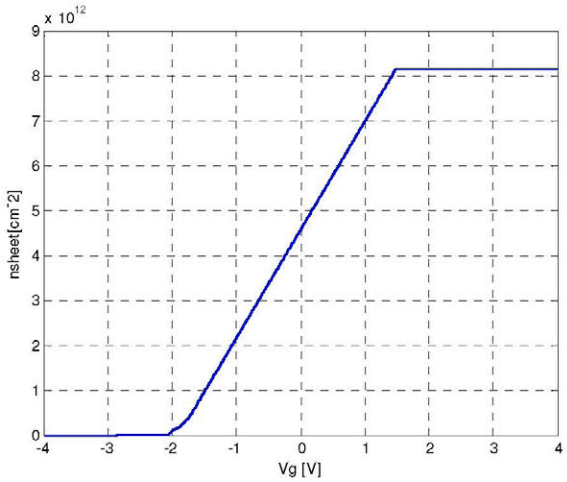

Figure 5. Variation of sheet carrier concentration with gate voltage

TABLE I. PHYSICAL PARAMETERS OF THE GAN FET

m [%]	L_{sd} [um]	W_g [mm]	L_g [um]	L_{gd} [um]	μ_n [cm^2/Vs]	d_{AlGaN} [nm]
18	6	120	2	4	1500	25

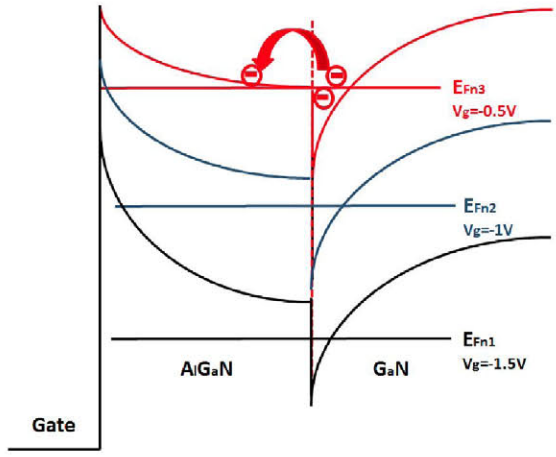

Figure 6. Conduction band diagrams for different gate voltages

Modeling of switch on-resistance, distinguishes three main components: the sheet resistance $R_{sh} = (q\mu_n n_s(V_g))^{-1}$ and the source and drain contact resistances (R_s and R_d, respectively) [12]. For a DEG channel, the on-resistance can be expressed by the following equation:

$$R_{on} = \frac{L_{sd}}{W_g} R_{sh} + R_s + R_d = \frac{L_{sd}}{W_g q \mu_n n_s(V_g)} + R_s + R_d \quad (1)$$

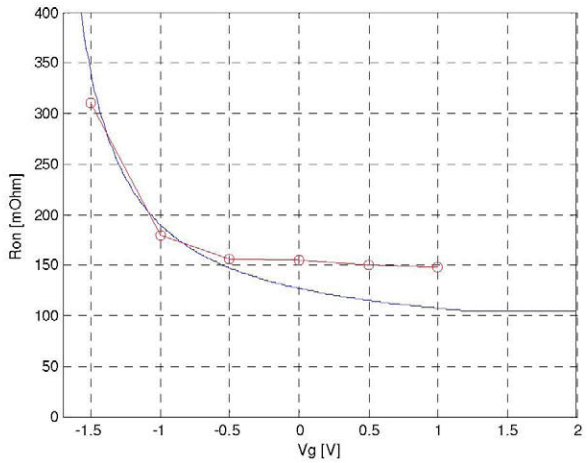

Figure 7. On-resistance dependence on the gate voltage: measured (red) and modeled (blue)

From the Fig. 7, it can be seen that there is a good agreement between the model and the measured values for R_{on} in low gate voltage range. For higher gate voltages, there is a higher difference between the measured and estimated values, since the model predicted saturation of the sheet density for gate voltages higher than 1.4V while experimentally this saturation already occurred at V_g=0V. This part of the model needs to be improved in the future work.

The drain current in the channel (in the linear part of the output characteristic) can be presented by the following equation [13]:

$$I_d = qW_g v(x) n_S(x) \quad (2)$$

where v(x) is the charge carrier (electron) drift velocity in the channel and can be presented by the following equation:

$$v(x) = \frac{\mu_n(V_g) E(x)}{1 + E(x)/E_C} \quad (3)$$

In (3), $\mu_n(V_g)$ is the carrier mobility which depends on the gate voltage, since for the higher values of V_g, parallel conduction path through AlGaN layer is being formed and overall mobility is being significantly decreased. Since this dependence has not been modeled yet, it was fitted according to experimental data (Fig. 8).

Equations (2) and (3) are valid only in non-saturation mode where the value for the electric field E(x) is lower than the critical value E_c. For higher values of V_{ds}, the channel pinches off from the drain and saturation of the drain current begins. Modeled and measured output characteristics of the HEMT are presented in Fig. 9.

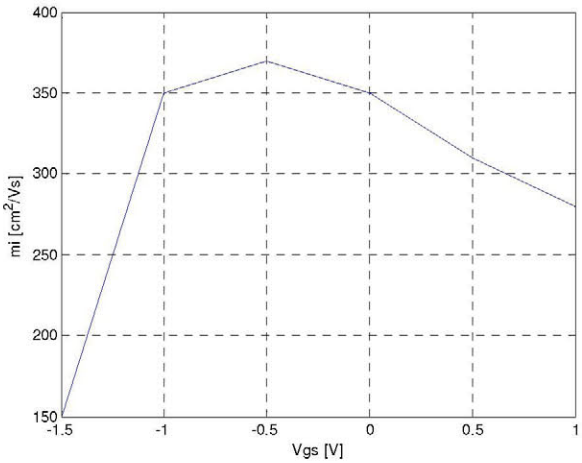

Figure 8. Fitted mobility dependence on the gate voltage

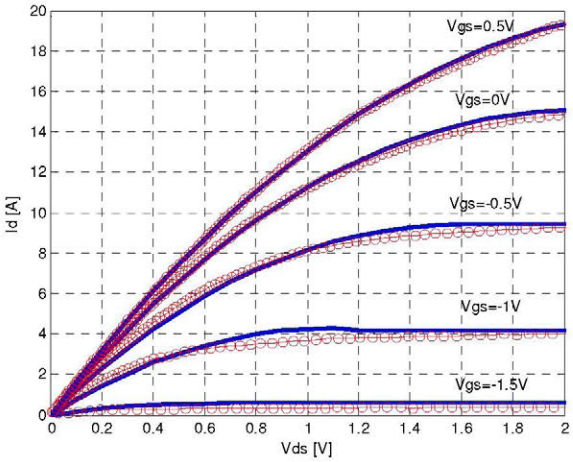

Figure 9. Measured (red dotted line) and modeled (blue line) variation of the drain current

It can be seen that there is a good agreement between the modeled and measured values, in linear and saturation region of operation. The main task in the future work is to avoid fitting of the mobility curve and model the conduction of the parasitic MESFET.

The gate capacitance characteristics are dominated by the variation of 2DEG density in the lower gate voltage region, while in the high gate voltage area, variation of ionized donor concentration due to donor neutralization and the contribution of free electrons in the AlGaN layer become important factors. In our model, only variation of 2DEG was taken into account, together with fringing and field plate capacitances [13]:

$$C_{gs} = qW_g L_g \frac{\partial n_{sheet}}{\partial V_g} + C_{fringing} + C_{fieldplate} \qquad (4)$$

The comparison between modeled and measured values for C_{gs} is presented in Fig. 10.

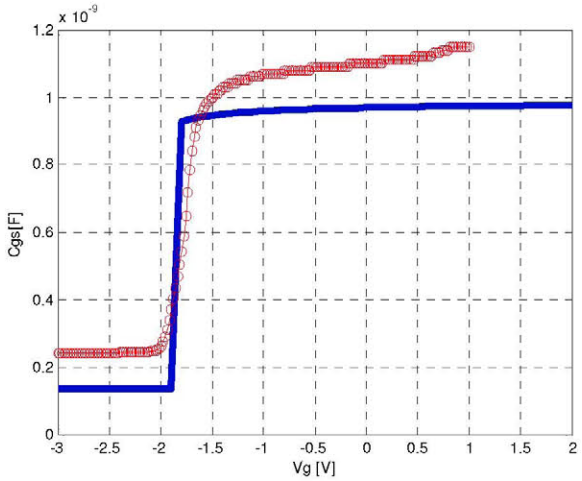

Figure 10. Measured (red) and modeled (blue) variation of C_{gs} with the gate voltage

It can be seen that modeled and measured C_{gs} dependences have the similar shape. Still, there is a difference between the estimated and measured values, especially in the region of higher gate voltages. The reason for this is negligence of neutralized donors and free AlGaN carriers contribution to the gate capacitance. Modeling of these factors will be one of the main tasks in the future work.

The input (C_{iss}=C_{gs}+C_{gd}), output (C_{oss}=C_{gd}+C_{ds}) and reverse transfer capacitance (C_{gd}) have been measured in the subthreshold regime for V_{GS}=-3V, changing the V_{DS} from 0 to the breakdown voltage of 100V, at frequency equal to 1MHz. The measured C-V curves are presented in Fig. 11.

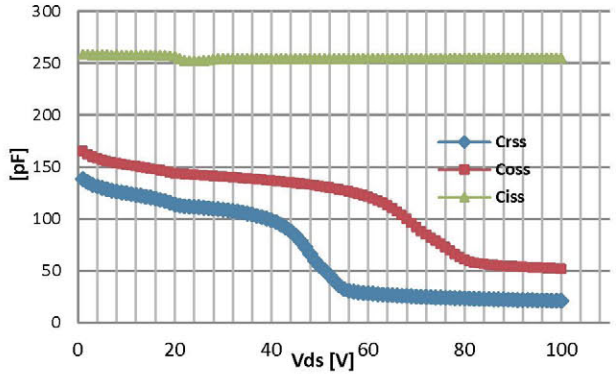

Figure 11. Measured C_{iss}, C_{oss} and C_{rss} of the FET at 1MHz

III. EXPERIMENTAL RESULTS

In this paper, the prototype of a simple buck converter with previously characterized IAF GaN HEMT was implemented and tested. The switching frequency was increased up to 25MHz for constant output power and 64QAM signal with approximately 1MHz of large signal bandwidth was generated at approximately 20MHz of the switching frequency.

Previous work demonstrated the advantages of commercially available GaN devices over Si MOSFETs in this kind of application. Our previous work showed that operation at switching frequency higher than 10MHz using EPC GaN HEMTs was not possible, because of the problems with power dissipation.

A. Implementation of the IAF prototype

Previously tested prototype with EPC1014 HEMTs which demonstrated the highest efficiency at high switching frequency, was implemented as a synchronous buck. IAF HEMT has the maximum on-resistance approximately equal to 180mΩ which is 11 times higher than R_{on} of EPC1014 and similar values for input capacitance C_{iss}, which means that Figure Of Merit (defined as a product of on-resistance and gate charge) of IAF HEMT is approximately 11 times worse [14]. But, it is important to emphasize that these devices have different current and voltage ratings (40V, 10A for EPC1014 and 100V, 27A for the IAF HEMT), so the comparison of FOMs is not completely adequate.

Anyhow, high on-resistance of the IAF devices implied that simple buck converter is more efficient solution than a synchronous one, since Schottky diode in parallel with the low-side switch is necessary because of the absence of the body diode in the design of the HEMT. The diode that was used in the design was low drop power Schottky diode, STPS20L25CT from ST microelectronics. The implemented prototype is presented in Fig. 12.

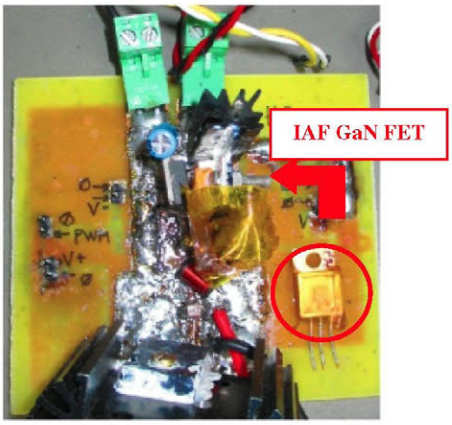

Figure 12. Implemented prototype with IAF GaN FET

B. Static characteristics comparison

The performance of the simple buck converter using IAF GaN device was tested at 4, 7, 10, 20 and 25MHz of the switching frequency, emulating the PA by the constant load resistance of 6Ω and changing the duty cycle in order to provide different power levels at the output. Input voltage was set to 24V. The efficiency curves for the two aforementioned EPC GaN prototypes, one prototype with Si MOSFETs with good FOM value and IAF prototype, at switching frequency of 7MHz are presented in Fig. 13. From these efficiency curves it can be seen that in the low power range (up to 25W), which is especially important for high

Peak to Average Power Ratio signals, the IAF prototype provided the second best result (after EPC1014), which was expected from the FOM value.

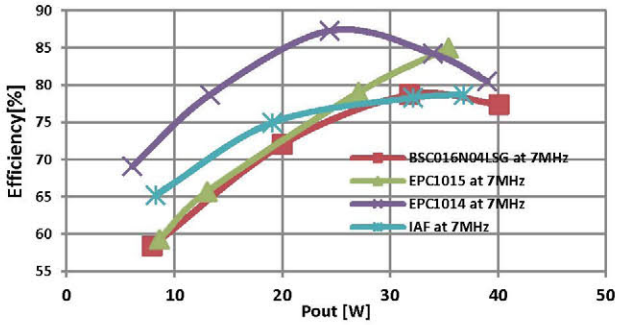

Figure 13. Comparison with the commercial devices at 7MHz

The prototypes with commercially available EPC 1014 and 1015 showed significantly worse thermal management and problems with power dissipation disabled the operation at switching frequency higher than 10MHz. The frequency increase up to 25MHz was possible with the IAF prototype and these efficiency curves are presented in Fig. 14.

C. *Power losses of IAF prototype-calculation and measurements*

In order to calculate the total power losses breakdown, the model from [15] modified for simple buck converter was implemented and compared with experimental results (Fig. 15). Since this simple model fits quite well in a low power range, it can be used for the total losses breakdown calculation. The total losses breakdown for P_{OUT}=12W at 15MHz is presented in Fig. 16. It showed that 76% of the total losses are switching losses in the IAF GaN HEMT.

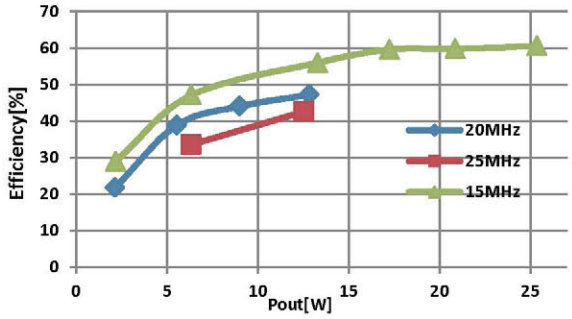

Figure 14. Efficiency curves for IAF prototype

D. *Thermal management comparison*

As it was previously mentioned, the prototypes with commercially available EPC 1014 and 1015 showed significantly worse thermal management and problems with power dissipation disabled the operation at switching frequency higher than 10MHz.

Application of IAF GaN HEMT provided more robust solution with better thermal management. The TO220 package of this device enabled putting and fixing the heat sink on the side of the HEMT which provided better heat extraction.

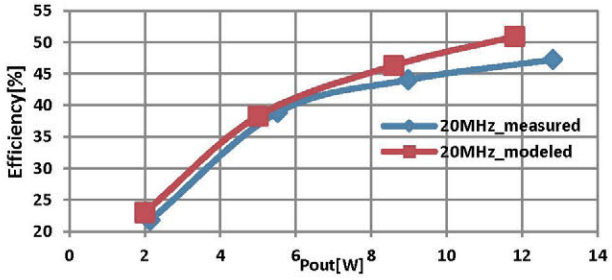

Figure 15. Efficiency model and measurements at 20MHz

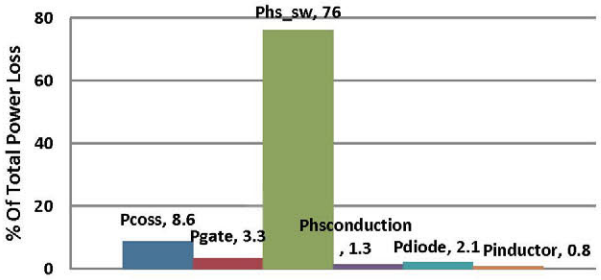

Figure 16. Percentage of the total losses model for 12W and 15MHz

In the case of LGA package of EPC devices the heat sink was on top of the devices, without possibility to be fixed, since the PCB layout was optimized for very high frequency with minimization of all parasitic loops. On the other hand, SiC substrate of IAF FET increased the overall thermal conductivity of the device and additionally improved the heat extraction process. Fig. 17 and 18 present thermal camera capture for EPC1015 and IAF prototype, operating at 10MHz with P_{OUT} approximately equal to 15W. The heat sink temperature of the IAF device increased up to 66 degrees while in the case of EPC1015, it reached even 120 degrees.

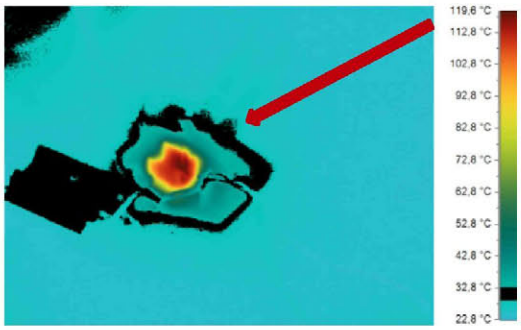

Figure 17. Thermal camera capture of EPC1015 prototype

E. *Dynamic tests comparison*

After the tests with the constant output power, 64QAM and WCDMA signals were generated, using the aforementioned prototypes. In order to make the performance comparison between EPC1014, EPC1015, Si BSC016N04LSG and IAF prototypes, the first generated envelopes had 250kHz of large signal bandwidth, applying the switching frequency of 5MHz, which is the lowest f_{sw} for generation of the aforementioned large signal bandwidth [7].

The average output power and efficiency values are presented in Table 2 and 3. The measured efficiency included losses in the driving circuit. As it was expected from the FOM values, the prototype with EPC 1014 devices demonstrated the highest efficiency.

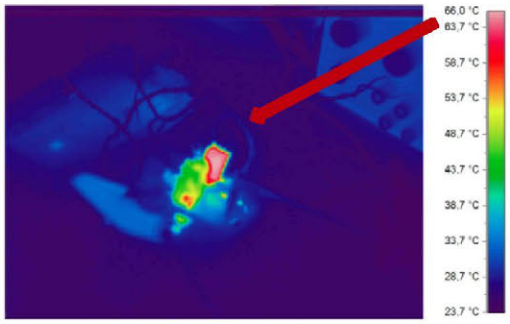

Figure 18. Thermal camera capture of IAF prototype

TABLE II. OBTAINED RESULTS FOR 64QAM WITH 250KHZ OF BW

64QAM R_{load} = 6Ω	EPC 1014	EPC 1015	BSC016N04LSG Si MOSFET	IAF GaN FET
$P_{out, avg}$[W]	14.3	13.6	12.3	12.9
Eff [%]	81.1	70.5	74.2	74.6

TABLE III. OBTAINED RESULTS FOR WCDMA WITH 250KHZ OF BW

WCDMA R_{load} = 6Ω	EPC 1014	EPC 1015	BSC016N04LSG Si MOSFET	IAF GaN FET
$P_{out, avg}$[W]	11.7	10.1	11.8	10.6
Eff [%]	80.9	69.8	70.8	71.4

Since the problems with power dissipation disabled the operation of EPC prototypes at 20MHz of switching frequency, 64QAM signal with approximately 1MHz of large signal bandwidth was generated only using the prototype with IAF FET (Fig. 19). The obtained efficiency for the average power equal to 5.4W and PAPR = 10.5dB was around 38%.

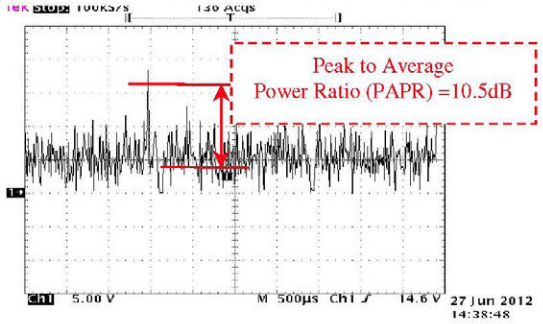

Figure 19. Generated 64QAM signal with 1MHz of BW

IV. CONCLUSIONS AND FUTURE WORK

The goal of this paper is implementation and testing of non-commercial GaN device in a simple buck converter for envelope amplifier in ET and EER transmission techniques. The implemented prototype provided better thermal management comparing to the prototypes with commercially available EPC1014 and 1015 devices. 64QAM signal with approximately 1MHz of large signal bandwidth and 10.5dB of PAPR was generated, operating at 20MHz of switching frequency. The proposed solution is suitable for increasing the large signal bandwidth processed by the switching part of the EA in the case of [8]. Also, there is a promising possibility for application in a multi-phase configuration [9], taking into consideration the wide large signal bandwidth and high PAPR obtained in this work.

In addition to this, some basic physical modeling has been done, in order to provide the correlation between the electrical characteristics of the GaN HEMT and physical design parameters. This is the first step in the optimization of the HEMT design for this particular application which is the main task in our future work.

REFERENCES

[1] H. Chireix, "High power outphasing modulation", Proc. IRE, vol. 23, no. 11, pp. 1370-1392, Nov. 1935

[2] K. Tom, K. Mouthaan, M. Faulkner, "Load Pull Analysis of Chireix Outphasing Class-E Power Amplifiers," in *Proc. IEEE Microwave Conference*, 2009, pp.2180-2183

[3] W. H. Doherty, "A New High- Efficiency Power Amplifier for Modulated Waves", Proc. IRE, vol. 24, no. 9, pp. 1163-1182, Sep. 1936

[4] J. Staudinger, B. Gilsdorf, D. Newman, G. Norris, G. Sadowniczak, R. Sherman, T. Quach, "High efficiency CDMA RF power amplifier using dynamic envelope tracking technique," Microwave Symposium Digest., IEEE, Vol. 2, June 2000, Pages: 873-876

[5] F. Wang, A. Yang, D. Kimball, L. Larson, P. Asbeck, "Design of a Wide-Bandwidth Envelope Tracking Power Amplifiers for OFDM Applications," *IEEE Trans. Microwave Theory and Techniques*, vol. 53, no. 4, pp. 1244-1255, April 2005

[6] C. Yu, A. Zhu, "A Single Envelope Modulator-Based Envelope Tracking Structure for Multiple-Input and Multiple-Output Wireless Transmitters," *IEEE Trans. Microwave Theory and Techniques*, vol. 60, no. 10, pp. 3317-3327, Oct. 2012

[7] F. H. Raab, "Intermodulation Distortion in Kahn- Technique Transmitters,"IEEE Transactions on Microwave Theory and Techniques, Volume 44, Issue 12, Part 1, December 1996, Pages 2273-2278

[8] F.Wang, D.F.Kimball, J.D.Popp, A.H.Yang, D.Y.Lie, P.M.Asbeck, L.E.Larson, "An Improved Power-Added Efficiency 19-dBm Hybrid Envelope Elimination and Restoration Power Amplifier for 802.11g WLAN Applications", IEEE Transactions on Microwave Theory and Techniques, Volume 54, Number 12, December 2006, pages 4086-4099.

[9] M. Norris, D. Maksimovic, "10 MHz Large Signal Bandwidth, 95% Efficient Power supply for 3G-4G Cell Phone Base Stations," in Proc. *IEEE APEC*, 2012, pp. 7-13

[10] Rashmi, A. Kranti, S. Haldar, R. S. Gupta, "An accurate charge control model for spontaneous and piezoelectric polarization dependent two-dimensional electron gas sheet charge density of lattice mismatched AlGaN/GaN HEMTs", *Solid-State Electronics*, Vol. 46, pp. 621-630, Nov 2001

[11] X. Cheng, M. Li, Y. Wang, "Physics-Based Compact Model for AlGaN/GaN MODFETs with Closed Formed I-V and C-V Characteristics", *IEEE Trans. Electron Devices*, vol. 56, no. 12, pp. 2881-2887, Decemberl 2009

[12] M. Esposto, A. Chini, S. Rajan, "Analytical Model for Power Switching GaN-Based HEMT Design", *IEEE Transactions on Electron Devices*, vol. 58, no. 5, May 2011

[13] M. K. Chattopadhyay, *Device Modeling of AlGaN/GaN High Electron Mobility Transistors (HEMTs)- an Analytical Approach*, Saarbrücken, Germany, LAP LAMBERT, 2010

[14] http://epc-co.com/epc/

[15] J. Klein, "Synchronous buck MOSFET loss calculations with Excel model", *App. Note AN-6005, Fairchild Semicond. Version 1. 0. 1*, 2006